JACS
JOURNAL OF THE AMERICAN CHEMICAL SOCIETY
Article
pubs.acs.org/JACS

Condensation of Methane in the Metal−Organic Framework IRMOF-1: Evidence for Two Critical Points

Nicolas Höft and Jürgen Horbach*

Institute for Theoretical Physics II, University of Düsseldorf, Universitätsstraße 1, 40225 Düsseldorf, Germany

Supporting Information

ABSTRACT: Extensive grand canonical Monte Carlo simulations in combination with successive umbrella sampling are used to investigate the condensation of methane in the nanoporous crystalline material IRMOF-1. Two different types of novel condensation transitions are found, each of them ending in a critical point: (i) a fluid−fluid transition at higher densities (the analog of the liquid−gas transition in the bulk) and (ii) a phase transition at low densities on the surface of the IRMOF-1 structure. The nature of these transitions is different from the usual capillary condensation in thin films and cylindrical pores where the coexisting phases are confined in one or two of the three spatial dimensions. In contrast to that, in IRMOF-1 the different phases can be described as bulk phases that are inhomogeneous due to the presence of the metal−organic framework. As a consequence, the condensation transitions in IRMOF-1 belong to the three-dimensional (3D) Ising universality class.

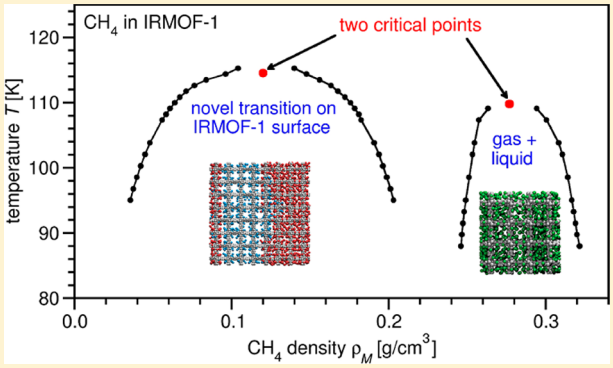

1. INTRODUCTION

The phase behavior of fluids in nanoscopic confinement has been associated with the exploration of novel phase transitions.[1−5] The interplay between wetting and surface transitions on homogeneous[3,6] as well as on chemically heterogeneous[7−9] substrates with different confined geometries leads to unique phenomena such as prewetting and layering transitions in thin films,[10,11] interface localization−delocalization,[3,4] the occurrence of fluid bridges between nanopatterned substrates,[12] or rounded phase transitions in cylindrical pores.[13] While the phase behavior of fluids in simple geometries such as thin films or cylindrical pores is well understood, the geometry and chemical structure of real porous media may be associated with novel phase transitions that have not been explored so far. As we reveal in this work, this is the case for metal−organic frameworks (MOFs).

MOFs form a broad class of porous materials which are highly stable and typically exhibit tailorable pore volumes of uniform size.[14−17] Due to their large inner surface, MOFs are well-suited for many applications[18] such as gas storage and separation,[19−23] catalysis,[24] chemical sensing,[25,26] and heat transformations.[27] A prototype of a MOF system is the isoreticular metal−organic framework IRMOF-1 where octahedral Zn−O−C clusters (in the following denoted as metallic centers) are linked together by organic groups, forming a three-dimensional (3D) nanoporous crystalline structure.[14,15] The structure of IRMOF-1 is different from other nanoporous materials such as zeolites[28] where the pores are typically cylindrical and thus gas molecules can be only adsorbed in preferred spatial direction. Instead, in IRMOFs the free pore volume forms an ordered 3D network. As we demonstrate in this work, condensation transitions in IRMOFs are fundamentally different from capillary condensation in cylindrical pores or thin films.

Previous experimental works[17,29−32] as well as computer simulation studies[33−37] have indicated that depending on temperature and pressure various arrangements of gas molecules in MOF structures such as IRMOF-1 are possible. If the density of the gas molecules is low, they are preferably located around the metallic centers. By gradually increasing the density of gas molecules, they tend to wet the surface of the whole framework. Eventually, with further increasing the density the MOF gets completely filled with gas molecules. The observation of the latter structures poses the natural question, whether they are also associated with phase transitions and the emergence of critical points. This is a nontrivial question since it is not clear a priori how two phases can coexist in the presence of the MOF framework. The small pore volume of a unit cell in IRMOF-1 does not allow for phase coexistence inside the unit cell. Thus, a phase transition in IRMOF-1 implies the existence of bulk phases, and each of these bulk phases is inhomogeneous due to the presence of the MOF framework. Moreover, two-dimensional (2D) interfaces between coexisting phases should form in the presence of the MOF structure. In fact, this is what we find in the present work

Received: April 20, 2015
Published: July 27, 2015

DOI: 10.1021/jacs.5b04077
J. Am. Chem. Soc. 2015, 137, 10199−10204

and surprisingly we observe the occurrence of two condensation transitions.

Several computer simulation studies using grand canonical Monte Carlo (GCMC) simulations of gases such as CO_2 and CH_4 in various IRMOFs have determined adsorption isotherms at low temperatures and found evidence for the emergence of a line of first-order phase transition ending in a critical point.[38−43] However, in none of the latter studies the coexisting phases have been characterized. Moreover, evidence has been given for only one condensation transition, and the applied simulation techniques did not allow to systematically explore the critical behavior and to study inhomogeneous systems where the coexisting phases are separated from each other by an interface.

We combine GCMC with successive umbrella sampling[44] and finite size scaling to elucidate the phase behavior of CH_4 in IRMOF-1. We find two types of condensation transitions, each of them ending in a critical point. The transition at high densities is the analog of the liquid−gas transition in pure CH_4, and thus we refer to it in the following as the IRMOF liquid−gas (ILG) transition. Note, however, that different from pure CH_4, the liquid as well as the gas phase are inhomogeneous, with an enrichment of CH_4 molecules on the framework of the MOF in both phases. The transition at low densities occurs on the surface of the IRMOF-1 framework and is due to the different interactions of CH_4 with the metallic centers on the one hand and the organic linkers on the other hand. In the following, this transition is denoted as IRMOF surface (IS) transition. We give evidence that the critical behavior in the vicinity of the critical points of the IS and the ILG transition belongs to the 3D Ising universality class. Furthermore, as we argue below, the occurrence of the two types of phase transitions is expected to be the generic case of gas adsorption in MOFs with a similar stability and structure as IRMOF-1.

A detailed knowledge of the phase diagram, as provided in this work for the condensation transitions of CH_4 in IRMOF-1, is necessary to design targeted functionalities of microporous materials such as MOFs. In fact, the occurrence of two phase transitions might be interesting for applications such as gas separation and storage of CH_4, using the remarkable feature of the IS and the ILG transition of CH_4 in IRMOF-1 that they occur in a very similar temperature range (with similar critical temperatures around 110 K).

2. METHODS

As in previous works,[35,36,40−43] IRMOF-1 is modeled as a rigid framework (cf. Figure 1) with fixed positions of C, H, Zn, and O atoms, as obtained from X-ray diffraction data.[14] Interactions between CH_4 molecules are described in terms of a single Lennard-Jones (LJ) potential.[46] LJ parameters for the interaction of CH_4 with the MOF atoms are extracted from the universal force field (UFF) model of Rappé et al.,[47] applying the Lorentz−Berthelot mixing rules to obtain the LJ cross interaction parameters. For this model, it has been shown[48] that good agreement with experiment is achieved with respect to methane adsorption isotherms at T = 298 K. In order to accelerate calculations of CH_4−MOF interactions, a pretabulated grid of the potential has been used to interpolate the potential using a 3D cubic Hermite polynomial interpolation scheme[49,50] with a spacing of 0.2 Å. The potential parameters as well as the cut-offs used for the different interaction potentials can be found in the Supporting Information.

In the GCMC simulations volume V, temperature T, and chemical potential μ, are fixed, while the total number of particles, N, fluctuates in accordance with trial insertions and removals of particles. As a result of the GCMC simulations, we obtain the histogram $H(N)$ that measures how often a system containing N particles is visited. The

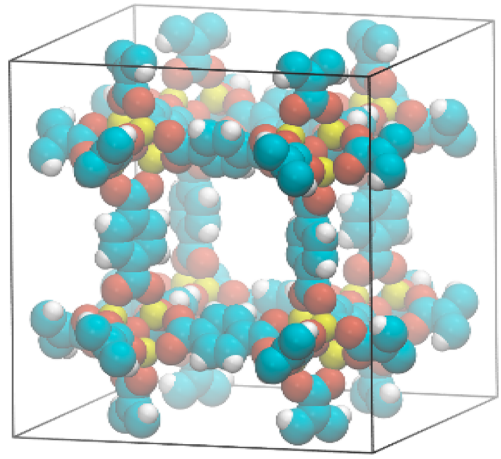

Figure 1. Unit cell of IRMOF-1. The spheres represent the different atoms, namely Zn (yellow), O (red), C (turquoise), and H (white).

normalization of $H(N)$ gives the probability distribution $P(N)$ (and thus the free energy of the system, $F(N) \propto -\log P(N)$ + const.). Successive umbrella sampling[44] is employed to enable an efficient sampling in the two-phase regions of the considered phase transitions where due to the formation of an interface between the coexisting phases the probability to sample these mixed-phase states compared to the pure phases is suppressed by a factor $\propto \exp[-\gamma A/k_BT]$ (with γ the interfacial free energy, A the total area of the interface, and k_B the Boltzmann constant). Similar to multicanonical sampling (see, e.g., ref 45 and references therein), successive umbrella sampling provides a biased sampling technique where instead of a simulation according to the original grand canonical distribution, sampling is performed according to an auxiliary distribution that allows to visit all states at a given chemical potential with the same probability, including those in the two-phase region. From the knowledge of the auxiliary distribution the original grand canonical distribution can be reconstructed by reweighting.

In successive umbrella sampling, the calculation of the histogram $H(N)$ is done in consecutive windows $n \in [N,N+1]$ (see ref 44). In each window, k_t trial insertions and removals of CH_4 molecules are performed; for the windows at large n, up to $k_t = 2 \times 10^7$ trial insertions and removals are used, while for small n, $k_t = 10^6$ is chosen. After 400 trial insertions and removals, a displacement cycle is applied to a given configuration of N particles, consisting of N trial displacements of a random particle with a maximal displacement of 0.67 Å.

The simulations are performed in cubic boxes with an edge length L, where L is a multiple of the linear dimension of the IRMOF-1 unit cell, L_{unit} = 25.669 Å. In the following, the considered system sizes range from 2^3 to 4^3 unit cells. In the case of the ILG transition, only systems with $L = 2L_{unit}$ and $L = 3L_{unit}$ were simulated, because very low acceptance probabilities of the order of 10^{-3} for trial insertions of particles did not allow the simulation of larger systems in this case. For comparison, we have also determined the phase diagram for the gas−liquid transition of bulk CH_4 using GCMC. The details of this simulation can be found in the Supporting Information. All the results are obtained from an average over 10 independent runs.

We would like to emphasize that in this work we perform state-of-the-art GCMC simulations that are computationally very expensive. The following examples may illustrate the computational load required for the calculations: For the ILG transition at T = 102 K and the system with 3^3 unit cells, the required CPU time was 68 days on an Intel Xeon IvyBridge E5-2697 (2.7 Ghz) using in each histogram bin 2×10^7 trial insertions and removals and 5×10^4 trial displacement moves. For the IS transition at T = 95 K and the system with 4^3 unit cells, the CPU time was 114 days on the same hardware using 4×10^6 trial insertion and removals and 10^4 trial displacement moves in each histogram bin.

DOI: 10.1021/jacs.5b04077
J. Am. Chem. Soc. 2015, 137, 10199−10204

3. RESULTS AND DISCUSSION

For a first-order phase transition, the probability distribution $P(N)$ at coexistence is bimodal, i.e., it exhibits two peaks at $N^{(1)}$ and $N^{(2)}$ that correspond to the densities of the coexisting phases, $\rho^{(1)} = N^{(1)}/V$ and $\rho^{(2)} = N^{(2)}/V$, respectively. Note that we have determined the coexistence chemical potential via histogram reweighting,[51] tuning the chemical potential such that the area under the two peaks in $P(N)$ is equal.[52,53] At a given temperature, the IS and the ILG transitions are seen at different chemical potentials (see Figure 3b). In both cases, the corresponding probability distributions $P(N)$ exhibit a two-peak structure where the equal area under both peaks accounts for the equal weight criterion for coexisting phases.[53]

The logarithm of coexistence probability distributions, log $P(N)$, as a function of the number of particles per unit cell at different temperatures below the critical temperature T_c is shown in Figure 2 for the IS transition (Figure 2a) and the ILG

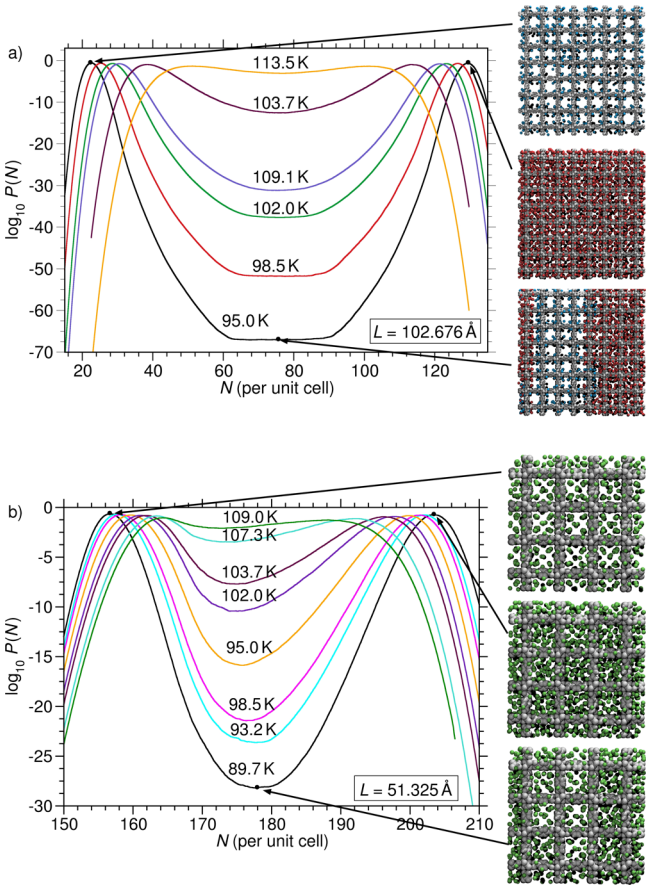

Figure 2. Logarithm of probability distribution $P(N)$ at different temperatures under coexistence conditions for (a) the IS phase transition and (b) the ILG phase transition. For the description of the snapshots, see text.

transition (Figure 2b). Data for the largest systems with linear dimension $L = 4L_{unit}$ for the IS transition and $L = 2L_{unit}$ for the ILG transition are displayed. The snapshots at $T = 95$ K for the IS and at $T = 89.7$ K for the ILG transition show configurations of the coexisting phases, including a configuration in the two-phase region in each case. The latter configurations indicate the occurrence of flat, 2D interfaces that separate the coexisting phases from each other.

From the probability distributions $P(N)$, one can directly obtain the binodals of the different phase transitions. Points on the binodals correspond to the location of the maxima of the probability distributions $P(N)$. In Figure 3a, the binodals are

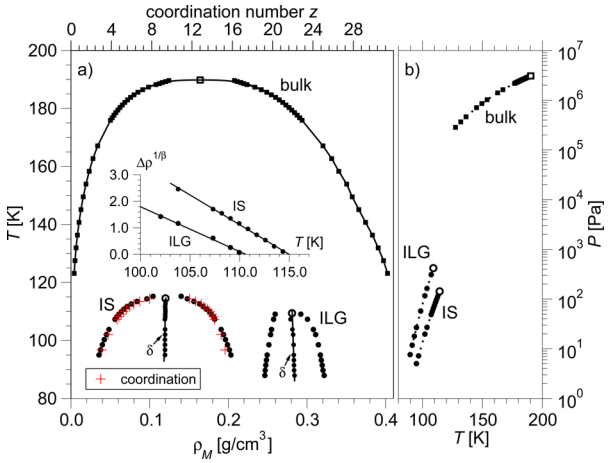

Figure 3. (a) Binodals of bulk CH_4 and of CH_4 in IRMOF-1 for the IS and ILG phase transition, as indicated. Red symbols (+) correspond to the coexistence temperatures as a function of the coordination number around the metallic centers (upper abscissa). As indicated, the plot also shows $\delta \equiv (\rho^{(1)} + \rho^{(2)})/2$ for the IS and the ILG transitions with fits to the coexistence diameter law (solid lines), see text. The inset shows rectification plot for the order parameter $\Delta\rho$ with $\beta = 0.324$, assuming 3D Ising universality (see text). Here, we have multiplied $(\Delta\rho)^{1/\beta}$ (with $\Delta\rho$ in units of g/cm^3) by the factors 10^3 and 10^4 for the IS and ILG transition, respectively. (b) Phase diagrams in the temperature−pressure plane. The critical points are shown as open symbols.

shown as a function of the mass density $\rho_M = NM_{CH_4}/V$, with $M_{CH_4} = 26.63 \times 10^{-24}$ g the mass of a CH_4 molecule (the definition of the coordination number, z, on the upper abscissa is given below). This plot also includes the binodals corresponding to the liquid−gas transition of bulk CH_4 with the critical temperature at $T_c = 190$ K and the critical density at $\rho_c = 0.16$ g/cm^3 (in good agreement with experiment[54]). The critical point for the ILG transition is at $T_c = 109.4$ K and $\rho_c = 0.28$ g/cm^3. These values are estimated from the binodal via the fits to the coexistence diameter law,[55] $\delta \equiv (\rho^{(1)} + \rho^{(2)})/2 = \rho_c + A_{rd}(T_c - T)/T_c)$ (with A_{rd} the rectilinear diameter), and the scaling law of the order parameter, $\Delta\rho \equiv \rho^{(2)} - \rho^{(1)} = A_{op}(T_c - T)/T_c)^{\beta}$ (with A_{op} a critical amplitude and $\beta = 0.324$, assuming 3D Ising universality).[57] Note that the quantity $\delta \equiv (\rho^{(1)} + \rho^{(2)})/2$ for the IS and the ILG transition with fits to the coexistence diameter law (solid lines) is included in Figure 3a. The inset of this figure shows a rectification plot for the order parameter $\Delta\rho$, i.e., $(\Delta\rho)^{1/\beta}$ (with $\beta = 0.324$) as a function of temperature. The critical point for the IS transition is at $T_c = 114.5$ K and $\rho_c = 0.12$ g/cm^3. While in this case we have also employed the coexistence diameter scaling to obtain ρ_c, the critical temperature T_c was determined by the Binder cumulant using the available data for different system sizes (see below).

Figure 3b shows the phase diagrams in the temperature−pressure plane. Note that in the GCMC the pressure P can be directly obtained from the chemical potential.[56] The IS as well as the ILG transitions are located in a pressure range between 1 Pa to 10^3 Pa, which is about 3 to 4 orders of magnitude below the pressure range of the bulk transition (cf. Figure 3b).

DOI: 10.1021/jacs.5b04077
J. Am. Chem. Soc. 2015, 137, 10199−10204

We estimate the critical temperature for the IS transition via the Binder cumulant,[58] defined by $U_L = 1 - (\langle\rho_M^4\rangle/3\langle\rho_M^2\rangle^2)$. Here, $\langle\rho_M^2\rangle$ and $\langle\rho_M^4\rangle$ are the second and fourth moment of the probability distribution $P(\rho_M)$, $\langle\rho_M^n\rangle = \int d\rho_M \rho_M^n P(\rho_M)$ with n = 2 and 4, respectively. In Figure 4, the cumulant U_L is plotted as

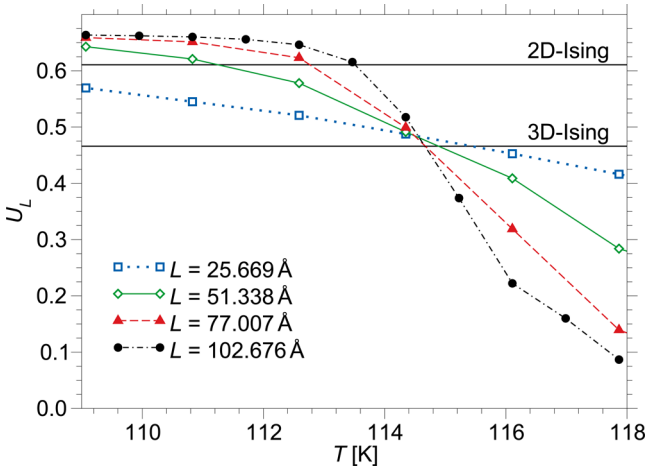

Figure 4. Temperature dependence of Binder cumulant, U_L, for different system sizes, as indicated. Horizontal lines indicate the universal values of U_L, as expected for the 2D and 3D Ising universality class.

a function of temperature (around T_c) for different system sizes, i.e., for different values of L. If L is sufficiently large, the curves for different L are expected to intersect at the critical temperature and a universal value of U_L which is $U_L^* = 0.61069$ for the 2D Ising[59] and $U_L^* = 0.4655$ for the 3D Ising universality class.[60] As can be inferred from Figure 4, the IS transition is consistent with 3D Ising universality; the small corrections to the universal value $U_L^* = 0.4655$ are expected due to finite size corrections.

While the ILG transition is the analog of the liquid–gas transition in the bulk, the IS transition is a phase transition occurring on the surface of the IRMOF-1 framework. The IS transition is due to the different interaction of the CH_4 with the metallic centers on the one hand and the organic linkers on the other hand. As a consequence, a low density surface phase appears where CH_4 molecules are preferably located around the metallic centers, and this phase coexists with a surface phase at higher densities where the whole framework is covered by CH_4. To characterize the two coexisting phases via a local order parameter, we have calculated the radial distribution function, $g_{met}(r)$, around the metallic centers, i.e., with respect to the oxygen atom located in the middle of the metallic center. This function describes, relative to an ideal gas, the probability of finding a CH_4 molecule at a distance r from the metallic center. As Figure 5 indicates for the two temperatures T = 96.7 and 110 K, the function $g_{met}(r)$ is clearly different for the two phases: The low density phase exhibits a double-peak structure for 4.0 < r < 7.0 Å, where the first peak corresponds to the shell of CH_4 molecules around the metallic center and the second one is due to the molecules adsorbed on the organic linker. Note that the first peak is essentially absent in $g_{met}(r)$ for the high density phase. For both phases, however, $g_{met}(r)$ is essentially zero for 7.0 < r < 9.0 Å, indicating that there are almost no molecules in the free pore volume. Note that we have checked that there are almost no particles in the free pore

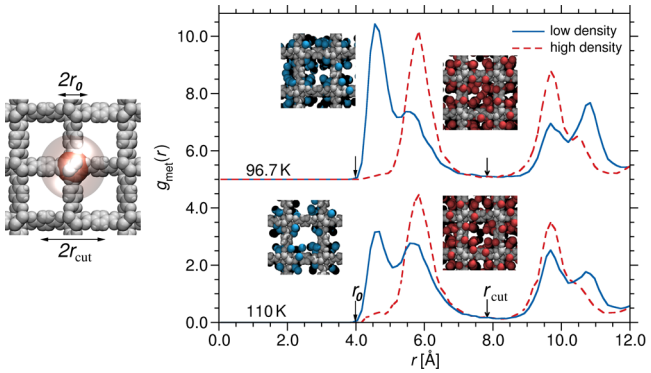

Figure 5. Radial distribution function $g_{met}(r)$ for the low density and high density phase of the IS phase transition at T = 110 and 96.7 K. The curves at the lower temperature are shifted by +5 on the ordinate. Also shown are snapshots of parts of the systems with the IRMOF-1 framework in gray and the CH_4 molecules as blue (red) spheres for the low density (high density) phase.

volume by explicitly counting them. When approaching the critical temperature, the amplitude of the first peak in $g_{met}(r)$ for the low density phase decreases, while relative to that the amplitude of the second peak increases. Thus, the function $g_{met}(r)$ for the low density phase becomes more equal to that of the high density phase when approaching T_c and they are, of course, identical at T_c.

Having analyzed the differences of $g_{met}(r)$ for the two phases, we can now introduce a coordination number z as a local order parameter, corresponding to the number of CH_4 molecules around a metallic center within a cutoff distance r_{cut} = 7.995 Å (cf. the schematic picture in Figure 5). That this local order parameter is sensible, is demonstrated in Figure 2a which shows that at least close to the critical point the two branches of z can be mapped onto the binodal of the IS transition (yielding a critical coordination number of z_c = 9.58). Thus, z can be used to locally distinguish between the low density and the high density phase of the IS transition. This is in particular helpful for the local identification of interfaces between coexisting IS phases.

4. CONCLUSIONS

We have performed extensive GCMC simulations in combination with successive umbrella sampling to study the condensation transitions of CH_4 in IRMOF-1. Two lines of transitions, each ending in a critical point, are found. These phase transitions are different from capillary condensation that has been considered in numerous studies of thin films and cylindrical pores. In IRMOF-1, inhomogeneous bulk phases coexist with each other, and interfaces between these bulk phases are formed that extend over the unit cells of the MOF structure.

Especially the IS transition is a novel phase transition that has not been explored so far. This transition is associated with the inhomogeneous 3D field exerted by the IRMOF-1 framework on the CH_4 molecules. Our analysis gives evidence that the IS transition belongs to the 3D Ising universality class. Furthermore, we have indicated the pressure range 1.0 < P < 10^3 Pa and a temperature range around 100 K where by the measurement of adsorption isotherms the IS and the ILG transition in IRMOF-1 could be found experimentally.

But are the IS and the ILG transitions also expected in other IRMOF structures? Other MOFs such as IRMOF-2, IRMOF-8,

DOI: 10.1021/jacs.5b04077
J. Am. Chem. Soc. 2015, 137, 10199–10204

IRMOF-10, or IRMOF-16 differ from IRMOF-1 essentially with respect to a larger length of the organic linkers and thereby they provide more "free volume" for the gas molecules. As we shall show in a forthcoming publication, more free volume leads to a broader coexistence range for the ILG transition. Furthermore, the IS transition is affected by the larger length of the organic linkers. On the one hand, for the CH_4 molecules the metallic centers are slightly more attractive than the organic linkers. On the other hand, the linkers "offer" more surface and therefore, for entropical reasons the CH_4 atoms are preferably adsorbed on the linkers. As a consequence, if the length of the linkers is increased (thus increasing also the pore volume such as in IRMOF-8 or IRMOF-16), the critical point for the IS transition shifts to lower temperatures.

However, both transitions are still present in other IRMOF structures. Moreover, similar condensation transitions, albeit in a different pressure/temperature range, are also expected for other gas molecules such as CO_2, N_2, and H_2O. Recent experiments and simulations have indicated that adsorption isotherms for these gases are qualitatively similar to those for CH_4. Thus, the occurrence of an IS and an ILG transition can be expected as the generic case for gas adsorption, at least in IRMOFs. The knowledge about the location of these transitions is important to taylor functionalities of MOFs with respect to gas adsorption. Note that experiments on the condensation transitions of methane in IRMOF-1 are currently under preparation.[61] An interesting question is also whether one observes similar phase transitions also in flexible MOF structures (for a model of such structures, see, e.g., ref 62). This will be a subject of forthcoming studies.

■ ASSOCIATED CONTENT

Supporting Information

The Supporting Information is available free of charge on the ACS Publications website at DOI: 10.1021/jacs.5b04077.

Details of the potential used for CH_4 in IRMOF-1 and of the calculation of the CH_4 bulk phase diagram (PDF)

■ AUTHOR INFORMATION

Corresponding Author

*horbach@thphy.uni-duesseldorf.de

Notes

The authors declare no competing financial interest.

■ ACKNOWLEDGMENTS

The authors thank Christoph Janiak and Bob Evans for useful discussions. The authors acknowledge financial support by Strategischer Forschungsfonds (SFF) of the University of Düsseldorf in the framework of the PoroSys network and by the German DFG, FOR 1394 (grant HO 2231/7-2). Computer time at the ZIM of the University of Düsseldorf is also gratefully acknowledged.

■ REFERENCES

(1) Dietrich, S. *J. Phys.: Condens. Matter* **1998**, *10*, 11469.
(2) Gelb, L. D.; Gubbins, K. E.; Radhakrishnan, R.; Sliwinska Bartkowiak, M. *Rep. Prog. Phys.* **1999**, *62*, 1573.
(3) Binder, K.; Landau, D.; Müller, M. *J. Stat. Phys.* **2003**, *110*, 1411.
(4) Binder, K.; Horbach, J.; Vink, R.; De Virgiliis, A. *Soft Matter* **2008**, *4*, 1555.
(5) Binder, K.; Virnau, P.; Statt, A. *J. Chem. Phys.* **2014**, *141*, 140901.
(6) Nakanishi, H.; Fisher, M. E. *Phys. Rev. Lett.* **1982**, *49*, 1565.
(7) Lenz, P.; Lipowsky, R. *Phys. Rev. Lett.* **1998**, *80*, 1920.
(8) Gau, H.; Herminghaus, S.; Lenz, P.; Lipowsky, R. *Science* **1999**, *283*, 46.
(9) Bauer, C.; Dietrich, S. *Phys. Rev. E: Stat. Phys., Plasmas, Fluids, Relat. Interdiscip. Top.* **1999**, *60*, 6919.
(10) Ball, P. C.; Evans, R. *J. Chem. Phys.* **1998**, *89*, 4412.
(11) Ball, P. C.; Evans, R. *Langmuir* **1989**, *5*, 714.
(12) Schoen, M. *Phys. Chem. Chem. Phys.* **2008**, *10*, 223.
(13) Wilms, D.; Winkler, A.; Virnau, P.; Binder, K. *Phys. Rev. Lett.* **2010**, *105*, 045701.
(14) Li, H.; Eddaoudi, M.; O'Keeffe, M.; Yaghi, O. M. *Nature* **1999**, *402*, 276.
(15) Eddaoudi, M.; Kim, J.; Rosi, N.; Vodak, D.; Wachter, J.; O'Keeffe, M.; Yaghi, O. M. *Science* **2002**, *295*, 469.
(16) Yaghi, O. M.; O'Keeffe, M.; Ockwig, N. W.; Chae, H. K.; Eddaoudi, M. *Nature* **2003**, *423*, 705.
(17) Rowsell, J. L. C.; Spencer, E. C.; Eckert, J.; Howard, J. A. K.; Yaghi, O. M. *Science* **2005**, *309*, 1350.
(18) Janiak, C.; Vieth, J. K. *New J. Chem.* **2010**, *34*, 2366.
(19) Janiak, C. *Dalton Trans.* **2003**, *14*, 2781.
(20) Dubbeldam, D.; Galvin, C. J.; Walton, K. S.; Ellis, D. E.; Snurr, R. Q. *J. Am. Chem. Soc.* **2008**, *130*, 10884.
(21) Li, J.-R.; Kuppler, R. J.; Zhou, H.-C. *Chem. Soc. Rev.* **2009**, *38*, 1477.
(22) Montoro, C.; Linares, F.; Procopio, E. Q.; Senkovska, I.; Kaskel, S.; Galli, S.; Masciocchi, N.; Barea, E.; Navarro, J. A. R. *J. Am. Chem. Soc.* **2011**, *133*, 11888.
(23) Yang, Q.; Liu, D.; Zhong, C.; Li, J.-R. *Chem. Rev.* **2013**, *113*, 8261.
(24) Lee, J. Y.; Farha, O. K.; Roberts, J.; Scheidt, K. A.; Nguyen, S. T.; Hupp, J. T. *Chem. Soc. Rev.* **2009**, *38*, 1450.
(25) Halder, G. J.; Kepert, C. J.; Moubaraki, B.; Murray, J. S.; Cashion, J. D. *Science* **2002**, *298*, 1762.
(26) Zeitler, T. R.; Allendorf, M. D.; Greathourse, J. A. *J. Phys. Chem. C* **2012**, *116*, 3492.
(27) Henninger, S. K.; Habib, H. A.; Janiak, C. *J. Am. Chem. Soc.* **2009**, *131*, 2776.
(28) Davis, M. E. *Nature* **2002**, *417*, 813.
(29) Rosi, N. L.; Eckert, J.; Eddaoudi, M.; Vodak, D. T.; Kim, J.; O'Keeffe, M.; Yaghi, O. M. *Science* **2003**, *300*, 1127.
(30) Yildirim, T.; Hartmann, M. R. *Phys. Rev. Lett.* **2005**, *95*, 215504.
(31) Siberio-Pérez, D. Y.; Wong-Foy, A. G.; Yaghi, O. M.; Matzger, A. *Chem. Mater.* **2007**, *19*, 3681.
(32) Uzun, A.; Keskin, S. *Prog. Surf. Sci.* **2014**, *89*, 56.
(33) Mueller, T.; Ceder, G. *J. Phys. Chem. B* **2005**, *109*, 17974.
(34) Walton, K. S.; Snurr, R. Q. *J. Am. Chem. Soc.* **2007**, *129*, 8552.
(35) Dubbeldam, D.; Frost, H.; Walton, K. S.; Snurr, R. Q. *Fluid Phase Equilib.* **2007**, *261*, 152.
(36) Liu, B.; Yang, Q.; Xue, C.; Zhong, C.; Chen, B.; Smit, B. *J. Phys. Chem. C* **2008**, *112*, 9854.
(37) Fairen-Jimenez, D.; Seaton, N. A.; Düren, T. *Langmuir* **2010**, *26*, 14694.
(38) Jiang, J.; Sandler, S. I. *Langmuir* **2006**, *22*, 5702.
(39) Walton, K. S.; Millward, A. R.; Dubbeldam, D.; Frost, H.; Low, J. J.; Yaghi, O. M.; Snurr, R. Q. *J. Am. Chem. Soc.* **2008**, *130*, 406.
(40) De Toni, M.; Pullumbi, P.; Coudert, F.-X.; Fuchs, A. H. *J. Phys. Chem. C* **2010**, *114*, 21631.
(41) Ma, Q.; Yang, Q.; Zhong, C.; Mi, J.; Liu, D. *Langmuir* **2010**, *26*, 5160.
(42) Hicks, J. M.; Desgranges, C.; Delhommelle, J. *J. Phys. Chem. C* **2012**, *116*, 22938.
(43) Desgranges, C.; Delhommelle, J. *J. Chem. Phys.* **2012**, *136*, 184108.
(44) Virnau, P.; Müller, M. *J. Chem. Phys.* **2004**, *120*, 10925.
(45) Janke, W. *Phys. A* **1998**, *254*, 164.
(46) Martin, M. G.; Siepmann, J. I. *J. Phys. Chem. B* **1998**, *102*, 2569.
(47) Rappé, A. K.; Casewit, C. J.; Colwell, K. S.; Goddard, W. A., III; Skiff, W. M. *J. Am. Chem. Soc.* **1992**, *114*, 10024.

DOI: 10.1021/jacs.5b04077
J. Am. Chem. Soc. 2015, 137, 10199−10204

(48) Düren, T.; Sarkisov, L.; Yaghi, O. M.; Snurr, R. Q. *Langmuir* **2004**, *20*, 2683.
(49) Schultz, M. H. *Spline Analysis*; Prentice-Hall: Englewood Cliffs, NJ, 1973.
(50) June, R. L.; Bell, A. T.; Theodorou, D. N. *J. Phys. Chem.* **1990**, *94*, 8232.
(51) Ferrenberg, A. M.; Swendsen, R. H. *Phys. Rev. Lett.* **1988**, *61*, 2635.
(52) Binder, K.; Landau, D. P. *Phys. Rev. B: Condens. Matter Mater. Phys.* **1984**, *30*, 1477.
(53) Borgs, C.; Kotecky, R. *J. Stat. Phys.* **1990**, *61*, 79.
(54) Friend, D. G.; Ely, J. F.; Ingham, H. *J. Phys. Chem. Ref. Data* **1989**, *18*, 583.
(55) The coexistence diameter also exhibits a singularity $\propto (T - T_c)^{1-\alpha}$ with $\alpha = 0.113$ for the 3D Ising universality class.[57] However, due to the smallness of the exponent α, this term is very similar to the regular linear term, and so we have not taken into account the singular term in the fits to the coexistence diameter.
(56) Frenkel, D.; Smit, B. *Understanding Molecular Simulation*, 2nd ed.; Academic Press: San Diego, CA, 2002.
(57) Pelissetto, A.; Vicari, E. *Phys. Rep.* **2002**, *368*, 549.
(58) Binder, K. *Z. Phys. B: Condens. Matter Quanta* **1981**, *43*, 119.
(59) Kamieniarz, G.; Blöte, H. W. J. *J. Phys. A: Math. Gen.* **1993**, *26*, 201.
(60) Luijten, E.; Fisher, M. E.; Panagiotopoulos, A. Z. *Phys. Rev. Lett.* **2002**, *88*, 185701.
(61) Janiak, C.; *private communication*.
(62) Coudert, F.-X.; Ortiz, A. U.; Haigis, V.; Bousquet, D.; Fuchs, A. H.; Ballandras, A.; Weber, G.; Bezverkhyy, I.; Geoffroy, N.; Bellat, J.-P.; Ortiz, G.; Chaplais, G.; Patarin, J.; Boutin, A. *J. Phys. Chem. C* **2014**, *118*, 5397.

DOI: 10.1021/jacs.5b04077
J. Am. Chem. Soc. 2015, 137, 10199−10204